14th International Conference on Structural Safety and Reliability - ICOSSAR'25
1-6 June, 2025 - Los Angeles California, USA
R. Ghanem, E. Johnson, S. Masri and A. Olivier (Eds)

DATA- AND SIMULATION-SUPPORTED SYSTEM RELIABILITY ASSESSMENT OF BRIDGES SUBJECTED TO EXTREME FLOODS AND CLIMATE CHANGE

SERGIO CASTRO-GIRALDO[12], TOBIAS FRIIS[2] AND SEBASTIAN THÖNS[3]

[1]Lund University
Lund, SE-221 00, Sweden
sergio_andres.castro_giraldo@kstr.lth.se
sebastian.thons@kstr.lth.se

[2]Rambøll Danmark A/S
2300 Copenhagen S
tfri@ramboll.dk

Key words: System Reliability, Extreme Flooding, Climate Change, Data-driven Engineering

Abstract. *The acknowledged high failure rate of bridges worldwide due to hydraulic events and its projected increase due to climate change imposes a significant challenge in bridge management. This study performs a system reliability assessment of a bridge subjected to extreme flooding events and climate change by integrating simulation discharge data and public databases. Considering different climate change scenarios, the bridge's failure probability is calculated along with its variability due to fluctuations in LQI-acceptability criteria. The results show that ignoring climate change can lead to overestimating the bridge's capacity, especially for scoured foundations. Furthermore, climate change affects not only the bridge's structural performance but also its acceptable failure probability. These findings highlight the need for a simulation- and data-driven system reliability assessment, along with a scenario-based evaluation of acceptable failure probabilities under climate change.*

1 INTRODUCTION

Historically, hydraulic actions on bridges, such as floods, scour, debris, and other water-driven phenomena, are reported to cause the highest number of bridge failures in several parts of the world [1]. For instance, in the United States, studies [3], [4] reported that hydraulic events caused 52% and 47% of bridge failures, respectively. Similar patterns of bridge failures are reported in India with 51% [4] and Turkey with 45% [5]. Although specific bridge failure data for Denmark has not been reported, studies estimate that floods and storms account for 38% and 32%, of the most prevalent disasters experienced in Europe, representing nearly USD 111.5 billion in economic losses [6]. The experienced losses highlight a growing concern since the frequency and severity of natural disasters will increase due to global warming [7].

Considering the significant impact of hydraulic events on bridges, it is important for decision-makers to evaluate the risk of bridge failure and assess the impact of climate change on this risk. However, decision-makers face several limitations during such assessments due to the lack of site-specific hydraulic and climate change data. Recent studies have evaluated

hydraulic risk on bridges considering climate change scenarios [8, 9], however, key factors such as risk acceptability and its variability due to climate change have not been addressed yet.

This paper addresses the aforementioned limitations in risk evaluation by introducing a novel approach for computing bridge failure probabilities due to hydraulic hazards, integrating simulation discharge data and system reliability analysis. Moreover, it presents how the acceptable failure probabilities vary when considering climate change. This is a relevant contribution since, in the context of Denmark and to the authors' knowledge, no study has assessed the impact of climate change on bridges while addressing its effects on risk acceptance.

In this paper, section 2 introduces the data type and sources used for the system reliability assessment for different climate change scenarios. This section also describes the methodology and discusses the concept of LQI-based risk acceptability and its related acceptable failure probabilities. Section 3 introduces the bridge case study, its associated loading, resistance and system model, and the computed failure probabilities and acceptable failure thresholds. Finally, section 4 presents the conclusions from this study.

2 DATA AND METHODS

2.1 Data description: simulation discharges and supporting databases

Over the years, Denmark has experienced an increase in the number of available public databases. For instance, observation and simulation discharge data from the Danish Hydrological Information and Forecasting System (HIP, for its Danish acronym) are intended to support decision-making for climate adaptation and planning in water management [10]. The HIP platform provides hydrological information (e.g., water levels, stream discharge, and shallow groundwater), covering both historical records and future projections. The projections used by the HIP follow the Representative Concentration Pathways (RCPs) [11]. The available hydrological information is generated through national hydrological models developed by the Danish Meteorological Institute (DMI) and the Geological Survey of Denmark and Greenland (GEUS). The most recent hydrological model in Denmark (HIP4Plus) was validated and calibrated with data from 308 hydrological stations, providing near-surface hydraulic calculations at a 500m and 100m resolution. For details on the hydrological model, see[12].

This study uses simulation discharge data from the HIP platform as input for the hazard modelling. Additionally, information about the structural and geotechnical properties of the bridge case study and Denmark's GDP and life expectancy at birth, is required for the reliability assessment. Table 1 describes the public data sources used in this study.

Table 1. Summary of public data sources and their application in this study

Data Type	Use	Source	Access
Stream Discharge: -Historical -Future projections	-Calculation of flooding events -Variability in projections of flooding events over different climate change scenarios	HIP4Plus (DMI)	[10]
Geotechnical	-Soil parameters for calculating foundation's capacity	Jupiter-database (GEUS)	[13]
Bridge Description	-Location, dimensions and characteristics of bridges	Road directory	[14]
Life Expectancy	-Computation of acceptable failure probabilities based on LQI criteria (see section 2.3)	IIASA	[15]
GDP Denmark			[16]

2.2 System reliability analysis under climate change

The gradual development of hydraulic actions on bridges depends, among other factors, on the flow discharge beneath the structure, which in turn defines the water height. This means that hydraulic actions will initially affect the bridge's foundation and substructure components, and as water rises, the superstructure can be compromised as well. Following this logic, for the system reliability analysis presented in this study, the bridge system is divided into two main sub-systems: (i) the substructure, which includes components such as piers, abutments and corresponding foundations (e.g., pile-groups) and (ii) the superstructure (e.g., bridge deck).

Therefore, for bridges exposed to hydraulic hazard under the influence of climate change, the failure probability of the bridge system $P(F_{system})$, can be calculated by modelling the sub-systems behaving as a series system, as follows:

$$P(F_{system} | H_j) = P\left(\left(F_{substructure} \cup F_{superstructure}\right) \middle| H_j\right) \quad (1)$$

where $F_{substructure}$ and $F_{superstructure}$ represents the failure event for both considered sub-systems, while H_j denotes the hydraulic hazard, represented by flooding events, whose likelihood is modeled with probability distributions for different flow discharges at the structure's location. The index j^{th} represents either historical discharge or future projected discharge associated to specific climate change scenarios (RCPs).

As previously mentioned, each sub-system is itself composed of several components, which can fail by specific mechanisms, such as structural failure (e.g., deck unseating due to hydraulic forces) or geotechnical failure (e.g., loss of vertical bearing capacity). Accordingly, at a component level, the failure probability is computed by using the corresponding component's limit state function (LSF). In a compact form, the failure probability for the i^{th} component and the j^{th} hydraulic hazard scenario, is computed as follows:

$$P(F_i) = P\left(g_i\left(D_{S_j}, Y_{W_j}\right)\right) = P\left(M_{R_i} \cdot R_i\left(D_{S_j}\right) - M_{S_i} \cdot S_i\left(Y_{W_j}\right) \leq 0\right) \quad (2)$$

where g_i represents the LSF, R_i and S_i are the resistance and loading models, and M_{R_i} and M_{S_i} are the corresponding model uncertainties. The loading model in the LSF depends on the water level (Y_{w_j}), which defines the magnitude of the hydraulic loads. Similarly, the resistance model depends on the damage state (D_{s_j}), resulting from an extreme flooding event.

Additionally, to accurately represent the relationship between components within a sub-system, their interaction can be modelled using logical or Daniels systems (for instance, [17]). The ductile Daniels system is particularly appropriate when the sub-system exhibits redundancy and ductile component behavior, allowing load redistribution among its components. In this context, the failure probability of the substructure is calculated by using a perfectly ductile Daniels system as:

$$P(F_{Substructure}) = P\left(M_{R_i} \sum_{i=1}^{n} R_i\left(D_{S_j}\right) - M_S \cdot S_S\left(Y_{W_j}\right) \leq 0\right) \quad (3)$$

where the sub-system loading and model uncertainty are denoted as S_S and M_S, respectively. The water level Y_{w_j} in previous equation is computed by using Manning's formula as:

$$Y_{w_j} = \left(\frac{n \cdot Q_j}{B \cdot s^{0.5}}\right)^{3/5} \tag{4}$$

where n is the Manning's roughness coefficient, B is the channel width, s is the slope of the channel and, Q_j is the flow discharge for the j^{th} hydraulic hazard scenario. For the current work, scour is the main damage mechanism, decreasing the resistance of the foundation within the substructure sub-system. The scour depth (Y_{st}) is computed as the combined scour effect caused by the pier, pile-cap, and pile-group [18], as presented below:

$$Y_{st_j} = \lambda_{st}[y_{pr} + y_{pc} + y_{pg}] \tag{5}$$

where y_{pr} y_{pc}, y_{pg} represent scour depth due to pier, pile-cap and pile-group, respectively. The uncertainty parameter λ_{st} accounts for the inherent uncertainties related to scour formula.

2.3 Acceptable failure probabilities

The acceptable failure probability is a quantitative measure of the maximum allowed failure rate of a structure in order to satisfy human safety requirements. Its calculation is derived from the broader concept of risk acceptability, which refers to the level of potential loss that individuals or society can tolerate. Similarly, authors such as [19] define risk acceptability as the level of risk achieved by the most acceptable alternative in a decision-making problem. Indeed, design guidelines recommend comparing probabilities of structural failure with the acceptable levels [20], [21], as shown in [22]. Acceptable risk levels can differ depending on the approach used for its formulation. However, the most common methodologies are based on the ALARP (As low as possible principle) and LQI (Life Quality Index) criteria. The latter is used in this study to derive acceptable failure probabilities.

The concept of LQI was initially proposed by [23] and became a widely accepted concept in academia and industry, as it describes how much should be invested in life-saving measures without affecting life quality. The LQI formulation involves two principal societal indicators: (i) gross domestic product (GDP) denoted as g and (ii) life expectancy at birth, l, as follows:

$$LQI = g^w l^{1-w} \tag{6}$$

where w is an estimate of time spend at work, as a fraction of life expectancy. For more information regarding the LQI principle, see [24]. The LQI invariance principle sets the foundation for the Societal Willingness to Pay (SWTP), an indicator of the maximum cost that society is willing to invest in saving a statistical life. Similarly, the Marginal Life Saving Cost (MLSC) concept defines the efficiency of a life saving measure, therefore, an efficient investment indicates that MLSC ≤ SWTP, complying with the societal needs. In the context of cost-benefit optimization [24], the LQI-based acceptability criteria, indicates a constrain as:

$$\frac{dC(p)}{dp} \geq -G_\Delta \cdot k \cdot N_{PE} \cdot \lambda \cdot \frac{dP_f(p)}{dp} \tag{7}$$

where $C(p)$ is a cost function depending on the decision parameter p, similarly for the acceptable failure probability $P_f(p)$. The factor λ is the arrival rate of the hazard modeled as a Poisson process; N_{PE} is the number of endangered people and k denotes the number of fatalities. The SWTP is included in the acceptability criteria through the factor G_Δ, which expresses in monetary terms how much society can afford for a unit mortality reduction [24], computed as:

$$G_\Delta = \frac{g}{q} \cdot C_\Delta(\rho, \delta) \tag{8}$$

where q is a fraction of the lifetime spent at work (w) and C_Δ is the increase of life expectancy with respect to mortality reductions, (accounting for discounting ρ, and age-averaging δ). Recent studies presented in [25] projected fluctuations in the GDP, a critical factor in the LQI-based acceptability criteria, this as a results of climate change. Therefore, it becomes essential to evaluate if the level of acceptable risks (e.g., derived from LQI) remains valid under variant climate conditions. This problematic was first introduced and practically illustrated in [26].

The present work addresses this issue by analyzing variations in acceptable failure probabilities under climate change scenarios, focusing on bridges subjected to flooding events.

3 CASE STUDY

Figure 1 presents the case study, a railway bridge in Jutland, Denmark, crossing the Storå River. The bridge carries a single railway track with a span length (L) of 11.25m and a total width of 5.3m. The superstructure is supported by a middle pier founded on piles placed in the river channel, while the ends are supported by abutments resting on shallow foundations.

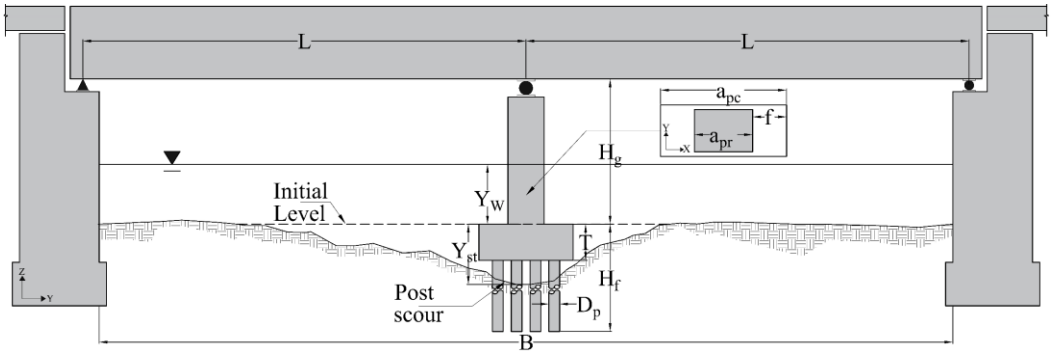

Figure 1. Geometrical layout of the bridge case study [14]. Initial level: riverbed level before scour occurs.

3.1 Flood frequency analysis

The simulated historical stream discharge Q, covering the period from 1989 to 2023, is used to generate Annual Maximum Series (AMS), which then are fitted to several probability distributions to determine the one that better represents the AMS data, especially in the tails. Both graphical (Q-Q plots) and quantitative goodness of fit tests (Anderson-Darling and Kolmogorov tests) are used to evaluate the fit, with the Pearson-III ($P3$) distribution leading to the best fit. The probability density function (PDF) for a $P3$ distribution is computed as follows:

$$Q \sim P3\,(\gamma, \alpha, \beta), \qquad f_Q(x) = \frac{1}{|\beta|\Gamma(\gamma)}\left[\frac{x-\alpha}{\beta}\right]^{\gamma-1} exp\left[-\frac{x-\alpha}{\beta}\right]$$
$$\mu = \alpha + \gamma\beta \qquad\qquad \sigma^2 = \beta\gamma^2 \tag{9}$$

where α, β and, γ represent the location, scale and shape parameters, respectively, and μ, σ, indicate mean and standard deviation. In a non-stationary scenario, the distribution parameters are expected to vary over time. While specific histograms of future discharge are unavailable, the HIP provides data on changes of mean and standard deviation of the historical discharge.

This is used to apply scenario-based changes to the historical mean and standard deviation as:

$$\mu_j = \mu_{hist}\left(\Delta_{\mu_j} \pm \varepsilon_{\mu_j}\right) \;\; ; \;\; \sigma_j = \sigma_{hist}\left(\Delta_{\sigma_j} \pm \varepsilon_{\sigma_j}\right) \tag{10}$$

where μ_{hist} and σ_{hist} are the mean and standard deviation from the fitted P3 distribution. The parameters $\Delta_{\mu_j}$and ε_{μ_j} indicate the projected change in the mean and its associated uncertainty for the j^{th} climate change scenario, while $\Delta_{\sigma_j}$and ε_{σ_j} correspond to the same quantities for the standard deviation. The final μ_j and σ_j are used to back-compute the distribution parameters and resulting PDFs, with uncertainty inclusion resulting in upper and lower bounds of Q. Figure 2 (a) shows the effect of climate change on the historical PDF of Q and the projected PDFs for one RCP scenario, while (b) shows the return levels of Q across all climate change scenarios.

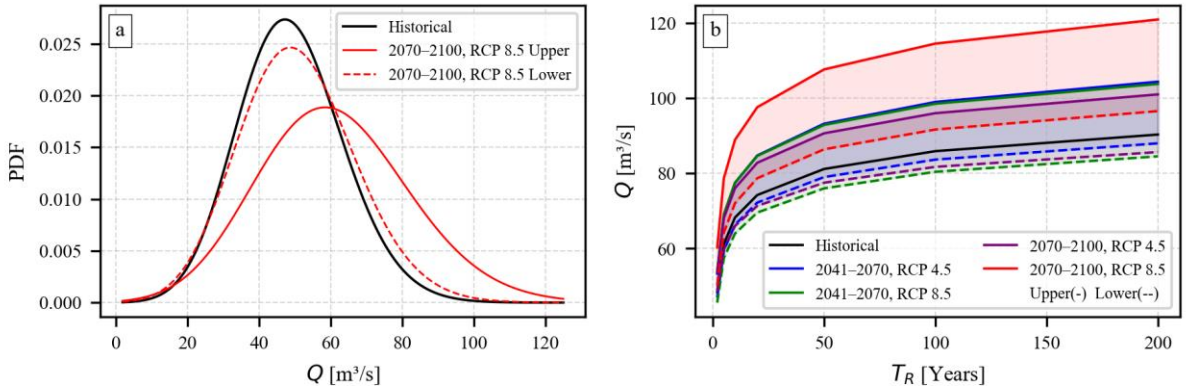

Figure 2. (a) PDFs of discharge Q for historical and lower and upper limit of RCP 8.5 scenario - 2070-2100, (b) flow discharge for different return periods and all the considered climate change scenarios (RCPs)

3.2 System reliability analysis

Based on the calculated flood magnitudes Q, Monte Carlo simulations are used to compute the water levels (Y_w, Eq. 4) and scour depths (Y_{st}, Eq. 5), with the parameters presented below:

Table 2. Description of variables used in the calculation of water level and scour depth

Variables			Distribution	Mean [μ]	CoV	Ref [μ, CoV]
Flow discharge	Q_j	[m³/s]	Pearson3	Figure 2		[10]
Channel width	B	[m]	Normal	23	0.05	[14, 27]
Scour uncertainty	λ_{st}	[-]	Normal	0.55	0.15	[28]
Manning's coefficient	n	[-]	LogNormal	0.035	0.28	[28]
Slope	s	[%]	LogNormal	0.096	0.05	[29, 30]
Shape factor	$K_{1_{pr}}$; $K_{1_{pc}}$	[-]	Deterministic	0.9; 1.1	-	[31]
Angle-attack factor	$K_{2_{pr}}$; $K_{2_{pc}}$	[-]	Deterministic	1	-	[31]
Riverbed factor	$K_{3_{pr}}$; $K_{3_{pc}}$	[-]	Uniform	1.1	0.05	[28]
Structural dimensions	$a_{pr}; a_{pc}; f\,; T$*	[m]	Normal	5.3;6;0.35;1	0.05	[14, 27]

*where: a_{pr} pier width a_{pc} pile-cap width, T pile-cap thickness, and f distance from pier edge to pile-cap

Using the simulated samples for scour depths (Y_{st}) and water levels (Y_w), it is possible to define the resistance and loading models, required for the system reliability analysis.

The substructure subsystem failure is modeled with geotechnical failure, representing the loss of vertical or lateral bearing capacity of the pile-group in the middle pier, while the superstructure subsystem is represented by the bridge deck (see, Figure 1). Building upon Eq. (1), the system failure probability for the case study is computed as follows:

$$P(F_{system} | H_j) = P\left((F_{foundation} \cup F_{bridge-deck}) \middle| H_j\right) \tag{11}$$

The failure probability of the foundation (pile-group) is calculated based on the definition of ductile Daniels system, where the overall resistance is computed as the sum of its individual pile resistances. For the presented case study, Eq. (3) takes the form of:

$$P(F_{foundation} | H_j) = P\left(M_{R_{V,H}} \cdot \sum_{i=1}^{N_p} R_{i_{V,H}}\left(D_{S_j}\right) - M_S \cdot S_S\left(Y_{W_j}\right) \leq 0\right) \tag{12}$$

where R_i and N_p indicate the induvial pile resistance and the total number of piles, respectively. The pile-group model uncertainty M_R represents the bias and the uncertainty between observed and predicted pile-group resistance, obtained from physical tests or numerical simulations (see Table 3). The subindexes V and H represent the direction of the resistance model, vertical or horizontal. For the individual pile resistance model (R_{i_V}), the vertical bearing capacity is composed of the shaft (q_s) and base resistance (q_b), which both among other parameters, dependent on the embedment of the pile. Consequently, this parameter is influenced by the scour depth (Y_{st}), reducing the pile's capacity. The individual vertical pile capacity (R_{i_V}) is calculated as follows:

$$R_{i_V} = q_b + q_s = A_b\left[\sigma'_V(Y_{st}) \cdot N_{q_{sand}}\right] + A_s\left[K_s \cdot \overline{\sigma'}_V(Y_{st}) \cdot \tan(\delta')\right] \tag{13}$$

where A_b is the base area, A_s is the surface area, $N_{q_{sand}}$ is the bearing capacity factor, K_s is the vertical to horizontal stress factor, and δ' represents the interface friction angle between the pile surface and the soil. The vertical and average vertical stresses depending on scour depth are denoted by $\sigma'_V(Y_{st})$, and $\overline{\sigma'}_V(Y_{st})$, respectively. The lateral resistance of a single pile (R_{i_H}) in a cohesionless soil is calculated following the approach presented in [32], as follows:

$$R_{i_H} = 0.3 \cdot \left[\chi' \cdot {K_p}^2 + \xi \cdot K_L\right] \cdot \tan(\delta') \cdot \gamma' \cdot a(Y_{st}) \cdot D_p \cdot [2.7 \cdot a(Y_{st}) - 1.7 \cdot L(Y_{st})] \tag{14}$$

where χ' is the shape factor, K_p and K_L are the passive and lateral earth pressure coefficients, ξ is resistance reduction factor, γ' is the effective soil's unit weight and D_p is the pile's diameter. In Eq. (14), both, the embedment length $L(Y_{st})$ and the rotation point $a(Y_{st})$ depend on scour.

For the superstructure it was verified that the water level reached during extreme events does not reach the bottom chord of the deck. Hence, the lateral resistance model for the deck is omitted, as the hydraulic load on the deck is extremely low (negligible failure probability).

Given that all piles share the same cross-section and installation process and considering a low local spatial variability of the soil, the resistances of the piles are modeled as fully correlated. Similarly, under an extreme flood, loads, damage states and failure modes (series system) are modeled as fully correlated. Lastly, considering that the same predictive models are utilized across all structural components, resistance and loading model uncertainties are modeled as fully correlated.

Table 3 presents the parameters used for the computation of resistance and loading models.

Table 3. Description of variables used in the calculation of bridge's system reliability

Variables			Distribution	Mean [μ]	CoV	Ref. [μ, CoV]
Resistance Parameters						
Soil unit weight	γ	[kN/m^3]	Normal	20*	0.05	[13, 33]
Soil friction angle	ϕ	[°]	Normal	35*	0.03	[13, 33]
Bearing capacity factor	$N_{q_{sand}}$	[-]	*Calculated*	30	-	-
Foundation Depth	H_f	[m]	Deterministic	Variable	-	-
Pile Diameter	D_p	[m]	Normal	0.3	0.05	[14, 27]
Number of piles	N_p	[-]	Deterministic	20	-	-
Group efficiency factor	M_{R_V} ; M_{R_H}	[-]	LogNormal	1.30 ; 0.4	0.21	[34, 35]
Loading Parameters						
Permanent load	G	[kN]	Normal	1593	0.05	[33]
Transient Load (train)	Q	[kN]	Gumbel	650	0.03	[33]
Lateral Hydraulic Load	$F_w(Y_w)$	[kN]	*Calculated*	Variable		[20]
Model Load Uncertainty	M_S	[-]	Normal	1	0.1	[33]

*Assumptions based on data obtained from a drilling hole located ≈30m from the middle pier's location [13]

No data was available regarding the middle pier foundation depth H_f. Therefore, this parameter is varied leading to range of foundation depths around the target reliability. Once resistance, load and correlation models are defined, the system reliability is computed using the parameters in Table 3, and by performing Monte Carlo simulations with $N_{samples} = 3 \times 10^7$. The results are presented in Figure 3, in terms of system reliability indexes (β_{sys}).

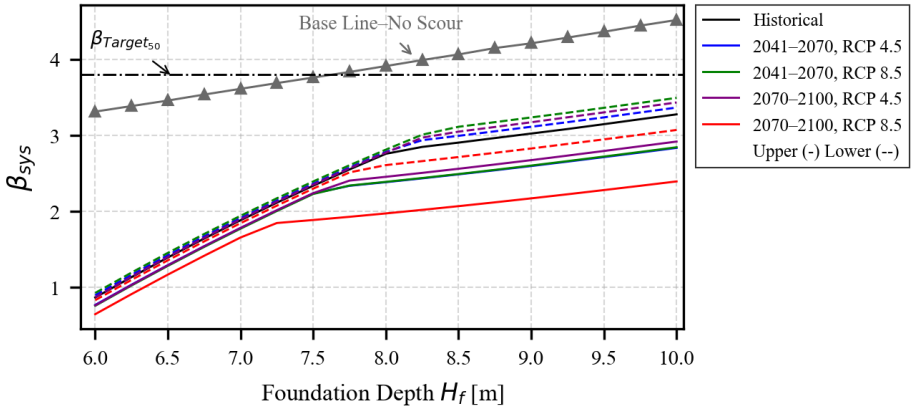

Figure 3. System reliability indexes for different foundation depths H_{f} across climate change scenarios. Vertical and horizontal failure modes as series system. The value of β_{Target} is extracted from [33] for CC2.

Figure 3 shows a significant reduction in the system reliability index when hydraulic loads and a scoured foundation are considered. For foundation depths less than ~10m and when considering scour effects, even the historical discharge can severely reduce the bridge's capacity, leading to reliability indexes lower than the target limit. This issue could be even more critical under high emission scenarios (RCP 8.5), where discharges are expected to increase. If no scour issues are considered, the foundation depth threshold, $\beta_{sys} < \beta_{Target}$, is ~7.6m.

The change in slope is attributed to the series system modelling, where the vertical LSF is

initially critical, and as foundation depth increases, the lateral LSF becomes critical. The previous results could guide foundation and scour inspections, helping to ensure that the critical reliability thresholds are met over the long term and under a variant climate condition.

3.3 Acceptable failure probability under Climate Change

This section is intended to illustrate that climate change not only affects the structural performance of the bridge but also it could alter the tolerance of society to risk failure. Building upon Eq. (8), the amount of money that society can invest in a life-safety measure may vary for different values of GDP. Therefore, the SWTP considering the j^{th} climate change scenario is:

$$G_{\Delta_j} = \frac{g_j}{q} \cdot C_{\Delta}(\rho, \delta) \tag{15}$$

Figure 4 presents the projected variation of GDP for Denmark [16], and the corresponding monetary SWTP over different Shared Socioeconomic Pathways (SSPs) [36].

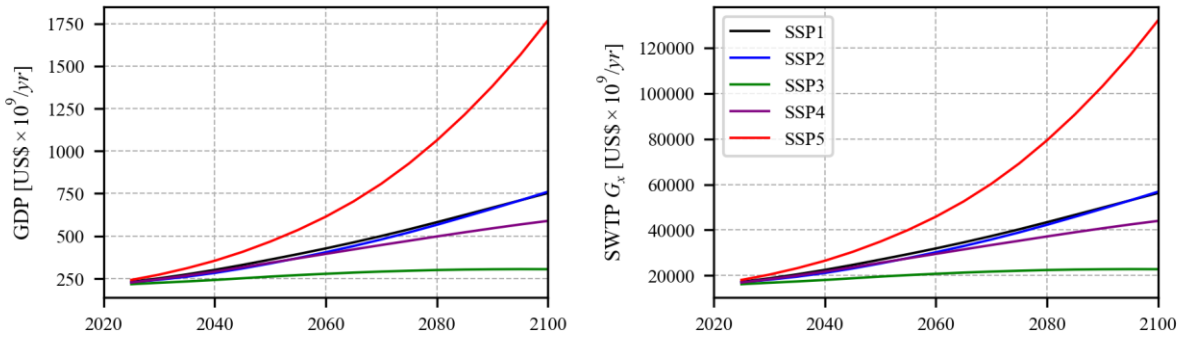

Figure 4. Variation of GDP per capita in billions adjusted to US$ in 2005 (left) [16], and SWTP over Shared Socioeconomic Pathways (SSPs) for Denmark

Although in previous sections, RCPs were used, due to data availability on the projected GDP, the risk acceptability is formulated based on SSPs. To address this, each RCP could be matched with a comparable SSP based on similar radiative forcing levels, as shown below:

Table 4. Approximate comparison of SSPs [36] and RCPs [11] with respect to radiative forcing

SSP	Summary description of SSPs	Rad. Forcing (W/m^2)	Related RCPs
SSP1	*Sustainability:* low challenges to mitigation-adaptation	5.0 – 5.8	RCP4.5 – RCP6.0
SSP2	*Middle:* medium challenges to mitigation-adaptation	6.5 – 7.3	
SSP3	*Regional-Rivalry:* high challenges to mitigation-adaptation	6.7 – 8.0	RCP6.0 – RCP8.5
SSP4	*Inequality:* low challenges to mitigation, high challenges to adaptation	6.0 – 8.3	
SSP5	*Fossil-fueled Development:* high challenges to mitigation, low challenges to adaptation	8.5 – 8.7	RCP 8.5

The LQI-based acceptability criteria presented in Eq. (7) shows that the cost of a risk reduction strategy and its corresponding failure probability depends on the decision parameter p. Considering that previous sections showed that scour damage could lead to an increase in the failure probability of the bridge, this illustrative example defines the decision

parameter as an increment in the resistance of the pile foundation, as: $R_{foundation}(1+p)$.

This illustrative example considers the vertical resistance model in Eq. (13), a specific foundation depth of 8 m and the simulated historical discharge Q (1989 to 2023) for estimating scour depths and hydraulic loads. For simplicity, these resistances and loading models are fitted to Normal distributions to estimate the projected change in acceptable failure probability. The cost of the risk reduction strategy is expressed as a function of the decision parameter p, as: $C(p) = 10^6 + 10^4 p^{1.25}$. The remaining involved parameters are retrieved from [37]. Solving the acceptability inequality presented in Eq. (7), for a scenario-based variation of the SWTP, the projected LQI-based acceptable P_f and β can be estimated, as presented in Figure 5.

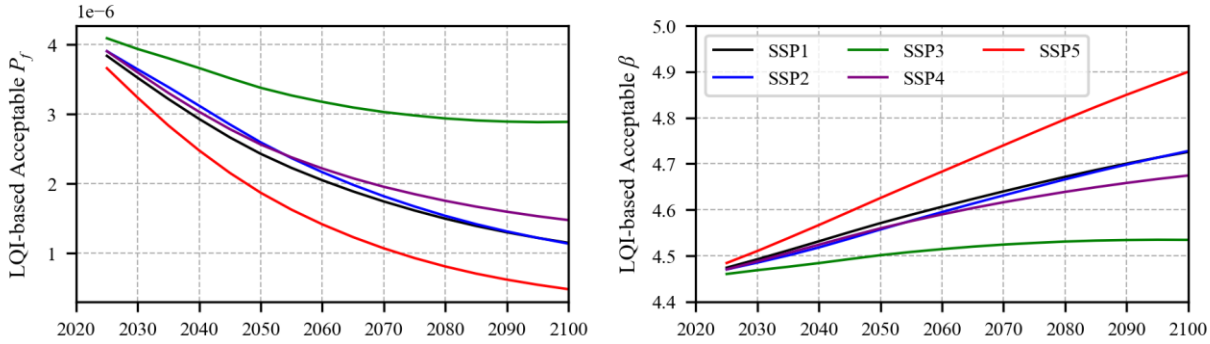

Figure 5. Projected LQI-based acceptable P_f and β index over different SSPs, considering the vertical LSF.

Figure 5 clearly shows that for SSP5; despite representing extremely high emissions, the associated GDP growth will lead to a higher capacity from society to invest in life safety, resulting in lower acceptable probabilities of failure and higher reliability indexes. In contrast, SSP3, showing lower increments in GDP, leads to a larger acceptable probability of failure from society. It is extremely important to mention that these findings do not suggest that high-emission scenarios should be pursued but rather highlight the dependency of risk acceptability on economic growth (e.g., GDP), a conclusion in line with the findings presented in [37].

4 CONCLUSIONS

Climate change represents a growing threat to existing and future infrastructure. This paper, based on system reliability assessment and its integration with public simulation discharge data, presented how to quantify the effect of global warming on a specific structure, indicating that extreme hydraulic events, even under a relatively small effect of climate change, induce a significant reduction in the bridge's safety. Additionally, the present work illustrates the sensitivity of LQI-based acceptable failure probabilities on economic growth, a factor strongly influenced by global warming. Furthermore, this paper shows the relevance of including public observation and simulation datasets in probabilistic flood risk assessments, facilitating the application of the data in real-world problems, and supporting decision-making under an uncertain hazard scenario due to global warming.

Acknowledgments. The authors gratefully acknowledge the financial support from the Bridgitise project (HORIZON-MSCA-2022-DN-01) and the Ramboll foundation.

REFERENCES

[1] W. Xiong, C. S. Cai, R. Zhang, H. Shi, and C. Xu, 'Review of Hydraulic Bridge Failures: Historical Statistic Analysis, Failure Modes, and Prediction Methods', *J. Bridge Eng*, Apr. 2023.

[2] K. Wardhana and F. C. Hadipriono, 'Analysis of Recent Bridge Failures in the United States', *J. Perform. Constr. Facil.*, vol. 17, no. 3, pp. 144–150, Aug. 2003.

[3] G. C. Lee, S. B. Mohan, C. Huang, and B. N. Fard, 'A Study of U.S. Bridge Failures (1980-2012)'.

[4] R. K. Garg, S. Chandra, and A. Kumar, 'Analysis of bridge failures in India from 1977 to 2017', *Structure and Infrastructure Engineering*, vol. 18, no. 3, pp. 295–312, Mar. 2022.

[5] H. S. Schaap and A. Caner, 'Bridge collapses in Turkey: causes and remedies', *Structure and Infrastructure Engineering*, vol. 18, no. 5, pp. 694–709, May 2022.

[6] Douris, James and Kim, Geunhye, *WMO Atlas of Mortality and Economic Losses from Weather, Climate and Water Extremes (1970–2019)*. Geneva, Switzerland: WMO: World Meteorological Organisation, 2021. Accessed: Dec. 03, 2024.

[7] K. Calvin *et al.*, 'IPCC, 2023: Climate Change 2023: Synthesis Report. Contribution of Working Groups I, II and III to the Sixth Assessment Report of the Intergovernmental Panel on Climate Change. IPCC, Geneva, Switzerland.', Intergovernmental Panel on Climate Change (IPCC), Jul. 2023.

[8] A. Nasr, I. Björnsson, and J. Johansson, 'National-Level Analysis of the Impact of Climate Change on Local Scour under Bridge Piers in Sweden', *J. Infrastruct. Syst.*, Jun. 2023.

[9] O. Khandel and M. Soliman, 'Integrated Framework for Quantifying the Effect of Climate Change on the Risk of Bridge Failure Due to Floods and Flood-Induced Scour', *J. Bridge Eng.*, vol. 24, no. 9, p. 04019090, Sep. 2019.

[10] HIP, 'Hydrological Information and Forecasting System'. Accessed: Dec. 19, 2024. [Online]. Available: https://hip.dataforsyningen.dk/

[11] D. P. Van Vuuren *et al.*,'The representative concentration pathways: an overview', *Climatic Change*, vol. 109, no. 1–2, Nov. 2011.

[12] H. Henriksen, S. Kragh, and J. Gotfredsen, *Development of nationwide model calculations of near-surface hydrological conditions in 100m grid using the dk model*.(GEUS), 2020. [Online]. Available: https://www.geus.dk.

[13] GEUS, 'Jupiter: National well database'. Accessed: Mar. 11, 2025. [Online]. Available: https://eng.geus.dk/products-services-facilities/data-and-maps/national-well-database-jupiter

[14] Vejdirektoratet, 'Danbro Web'. Accessed: Apr. 10, 2025. [Online]. Available: https://danbroweb.vd.dk/Danbro/

[15] W. C. for Demography and G. H. Capital, 'Wittgenstein Centre Data Explorer (WCDE v3)'. [Online]. Available: https://dataexplorer.wittgensteincentre.org/wcde-v3/

[16] International Institute for Applied Systems Analysis, 'IIASA SSP Database'. Accessed: Mar. 01, 2025. [Online]. Available: https://tntcat.iiasa.ac.at/SspDb/dsd?Action=htmlpage&page=10#intro

[17] S. Celati, A. Natali, W. Salvatore, and S. Thöns, 'System reliability accounting for corrosion-induced degradation over time', presented at the IABSE Symposium, Manchester 2024.

[18] J. S. Jones and D. M. Sheppard, 'Local Scour at Complex Pier Geometries', in *Building Partnerships*, Minneapolis, Minnesota, United States: American Society of Civil Engineers, Sep. 2000.

[19] B. Fischhoff, S. Lichtenstein, P. Slovic, R. Keeney, and S. Derby, 'Approaches to acceptable risk: a critical guide', Dec. 1980. .
[20] *EN 1991-1-7: Eurocode 1: Actions on structures - Part 1-7: General actions - Accidental actions*. Brussels: CEN, 2006.
[21] Joint Committee on Structural Safety (JCSS), *The JCSS probabilistic model code*. 2001.
[22] S. Thöns and M. G. Stewart, 'On the cost-efficiency, significance and effectiveness of terrorism risk reduction strategies for buildings', *Structural Safety*, vol. 85, Jul. 2020.
[23] J. S. Nathwani, N. C. Lind, and M. D. Pandey, *Affordable Safety by Choice- the Life Quality Method*. Inst. for Risk Research, University of Waterloo, 1997.
[24] R. Rackwitz, 'The Philosophy Behind the Life Quality Index and Empirical Verification', *Updated memorandum to JCSS, Technical University Munich*, 2005.
[25] T. Kompas, V. H. Pham, and T. N. Che, 'The Effects of Climate Change on GDP by Country and the Global Economic Gains From Complying With the Paris Climate Accord', *Earth's Future*, vol. 6, no. 8, pp. 1153–1173, Aug. 2018.
[26] A. Nasr, O. L. Ivanov, I. Björnsson, and J. Johansson, 'The need for nonuniform risk acceptability across climate change scenarios', *Risk Analysis*, vol. n/a, no. n/a, Mar. 2024.
[27] D. Seo, S. Shin, and B. Han, 'Reliability-based Structural Safety Evaluation of Reinforced Concrete Members', *Journal of Asian Architecture and Building Engineering*, vol. 9, no. 2, pp. 471–478, Nov. 2010.
[28] Ghosn, Michel, J. Wang, and F. Moses, *Design of Highway Bridges for Extreme Events-NCHRP Report 489*. Washington, DC: National Research Council (U.S.). Transportation Research Board, 2003.
[29] Scalable Algorithmics (SCALGO), *SCALGO Live*. (2024). [Online]. Available: https://scalgo.com/live
[30] M. Ghosn, F. Moses, and J. Wang, *Design of highway bridges for extreme events*. in NCHRP report, no. 489. Washington, D.C: Transportation Research Board, 2003.
[31] L. A. Arneson, L. W. Zevenbergen, P. F. Lagasse, P. E. Clopper, and Ayres Associates, *Evaluating Scour at Bridges: Fifth Edition*. National Highway Institute (U.S.), 2012. Accessed: Feb. 04, 2025. [Online]. Available: https://rosap.ntl.bts.gov/view/dot/42053
[32] Y. V. S. N. Prasad and T. R. Chari, 'Lateral Capacity of Model Rigid Piles in Cohesionless Soils', *Soils and Foundations*, vol. 39, no. 2, pp. 21–29, Apr. 1999.
[33] B. Van den Eijnden *et al.*, Eds., *Reliability-based verification of limit states for geotechnical structures: guidelines for the application of the 2nd generation of Eurocode 7: geotechnical design*. Luxembourg: Publications Office, 2024.
[34] L. Zhang, W. H. Tang, and C. W. W. Ng, 'Reliability of Axially Loaded Driven Pile Groups', *J. Geotech. Geoenviron. Eng.*, vol. 127, no. 12, pp. 1051–1060, Dec. 2001.
[35] E. A. Elgridly, A. L. Fayed, and A. A. A.-F. Ali, 'Efficiency of pile groups in sand soil under lateral static loads', *Innov. Infrastruct. Solut.*, vol. 7, no. 1, p. 26, Feb. 2022.
[36] K. Riahi *et al.*, 'The Shared Socioeconomic Pathways and their energy, land use, and greenhouse gas emissions implications: An overview', *Global Environmental Change*, vol. 42, pp. 153–168, Jan. 2017.
[37] H. Streicher and R. Rackwitz, 'Optimization with a LQI Acceptance Criterion'.